

Conversion of left ventricular endocardial positions from patient-independent co-ordinates into biplane fluoroscopic projections

M. Potse¹ R. Hoekema² A. C. Linnenbank^{3,4} A. SippensGroenewegen⁵
J. Strackee¹ J. M. T. de Bakker^{4,6} C. A. Grimbergen^{1,7}

¹Medical Physics Department, Academic Medical Center, Amsterdam, The Netherlands.

²Clinical Neurophysiology Department, University Medical Center, Utrecht, The Netherlands

³Heart Lung Center Utrecht, Utrecht, The Netherlands

⁴Experimental and Molecular Cardiology Group, Cardiovascular Research Institute, Academic Medical Center, Amsterdam, The Netherlands

⁵Cardiac Focus Inc., Pleasanton, CA, USA

⁶ICIN, Utrecht, The Netherlands

⁷Control Department, Faculty of Design, Construction, and Production, Delft University of Technology, Delft, The Netherlands.

Abstract — *Electrocardiographic body surface mapping is used clinically to guide catheter ablation of cardiac arrhythmias by providing an estimate of the site of origin of an arrhythmia. The localisation methods used in our group produce results in left-ventricular cylinder co-ordinates (LVCCs), which are patient-independent but hard to interpret during catheterisation in the electrophysiology laboratory. It is preferable to provide these results as three-dimensional (3D) co-ordinates, which can be presented as projections in the biplane fluoroscopic views that are used routinely to monitor the catheter position. We investigated how well LVCC can be converted into fluoroscopic projections with the limited anatomical data available in contemporary clinical practice. Endocardial surfaces from magnetic resonance imaging (MRI) scans of 24 healthy volunteers were used to create an appropriate model of the left-ventricular endocardial wall. Methods for estimation of model parameters from biplane fluoroscopic images were evaluated using simulated biplane data created from these surfaces. In addition, the conversion method was evaluated using 107 catheter positions obtained from eight patients, by computing LVCC from biplane fluoroscopic images and reconstructing the 3D positions using the model. The median 3D distance between reconstructed positions and measured positions was 4.3 mm.*

Keywords — *Endocardial catheter mapping, Body surface mapping, Catheter ablation, Biplane fluoroscopy, MRI*

Med. Biol. Eng. Comput., 2001, 40, 41–46

1 Introduction

ELECTROCARDIOGRAPHIC BODY SURFACE MAPPING provides noninvasive localisation of supraventricular and ventricular arrhythmias, which may be used to guide and direct catheter mapping prior to radiofrequency ablation (DUBUC *et al.*, 1993; PEETERS *et al.*, 1999).

A frequently applied method for such electrocardiographic localisation is based on the use of the QRS integral map (QRSI) of a single beat of a ventricular arrhythmia. This QRSI is compared with a previously collected database of QRISs corresponding to known pacing segments (SIPPENSGROENEWE-

GEN *et al.*, 1990; 1992), and the site of origin is then predicted as the segment corresponding to the best-matching QRSI in the database.

To make comparisons between subjects possible, and to allow generalisation to patients with different ventricular geometry, the database segment positions have been expressed in patient-independent 'left-ventricular cylinder co-ordinates' (LVCCs) (SIPPENSGROENEWEGEN *et al.*, 1990). These co-ordinates are usually presented in a polar plot (Fig. 1). A recently developed method provides a continuous estimate of the site of origin in the left ventricle using the LVCC system (POTSE *et al.*, 2000).

During a catheter ablation procedure, the physician observes the heart and catheter position using biplane fluoroscopy. To move the catheter to the estimated site of origin of an arrhythmia in the left ventricle, he/she has to convert the catheter-displacement advice obtained from the ECG to the anatomical

Correspondence should be addressed to Dr M. Potse;
e-mail: M.Potse@amc.uva.nl

Paper received 7 June 2001 and in final form 27 September 2001

MBEC online number: 20013625

© IFMBE: 2002

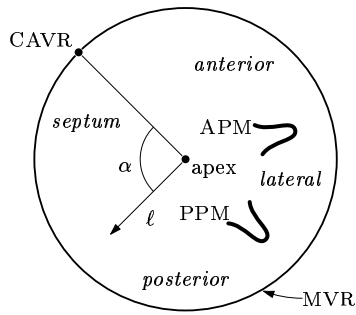


Fig. 1 Left-ventricular polar projection illustrating LVCCs. Apex of left ventricle is indicated in middle of diagram; circumference represents mitral valve ring (MVR). Centre of aortic valve ring (CAVR) is indicated. LVCCs consist of relative length l , indicating distance along apex–MVR axis relative to length of this axis, and azimuth α , defined with respect to position of CAVR

picture that he/she has in mind, while translating this picture to fluoroscopic projections. These are demanding tasks, given the mass of information that requires simultaneous apprehension in the electrophysiology laboratory, and they are necessarily subjective. It is preferable to present estimated positions directly in the biplane fluoroscopic images. For our localisation methods, this requires conversion of LVCCs to fluoroscopic projections.

If the positions of the X-ray sources and detectors are known, fluoroscopic projections of points in space can be created from their three-dimensional (3D) co-ordinates. The 3D co-ordinates of points on the left-ventricular (LV) endocardial wall in turn can be computed from LVCC by projection on the wall, if the wall geometry is accurately known and if each cross-section of the wall perpendicular to the apex–mitral valve ring axis is star-like with respect to the intersection point with the axis, i.e., any half-line that originates in the axis and runs perpendicular to it, intersects the endocardium exactly once. We assume that in the left ventricle the deviations from a star-like shape are small enough to be ignored for our purposes.

The LV wall geometry of a particular patient is usually not accurately known. In most cases, at best, endocardial contours obtained by contrast ventriculography are available during a catheter ablation procedure. Therefore we investigated construction of fluoroscopic projections from LVCC with a simple model for which all the required parameters can be obtained from the biplane images.

Based on visual inspection of magnetic resonance imaging (MRI) data of the hearts of 24 healthy subjects, we created two models to describe the left-ventricular wall:

model 1: a full ellipsoid of revolution of which only a part is used

model 2: a half ellipsoid of revolution.

We studied the ability of these two models to describe the LV wall geometry by fitting them to the MRI data. Secondly, we studied whether their parameters can be estimated from biplane fluoroscopic projections of the heart. These projections were simulated from the MRI data. Finally, we tested the application of the second model for conversion from LVCC into fluoroscopic projections using both the MRI data and actual biplane images obtained during cardiac catheterisation.

2 Materials

Geometric data of the LV endocardial wall were obtained from MR images of 24 healthy subjects (14 male and ten female).

Their age ranged from 22 to 64 years. The MRI scanner used was a 1.5 T Siemens Magnetom SP. The scanned MR images were based on standard echocardiographic imaging views, perpendicular to the so-called ‘long axis of the heart’ (BURBANK *et al.*, 1988). This axis runs approximately parallel to the line from the LV apex to the middle of the mitral valve ring (MVR). The long axis of the heart is indicated schematically in Fig. 2. Images perpendicular to this axis are called ‘short-axis images.’

For each subject, the long axis of the heart was selected using the procedure described by BURBANK *et al.* (1988) (HOEKEMA *et al.*, 1999) and the heart was imaged using about 12 short-axis images at 10 mm distances (Turbo-flash sequence). An example is shown in Fig. 2. To minimise movement artifacts, these images were produced during end-diastole by triggering on the peak of the R wave of the ECG, with the subject holding his breath. The contours of the LV endocardium (the inner surface of the LV) were discretised from the MR images using dedicated segmentation software. A triangulated representation of the endocardium was constructed from these contours. The resulting triangulations consisted of 85 ± 17 vertices (range 55–120, depending on the size of the ventricle).

To test clinical applicability, we also used 107 catheter positions measured with biplane fluoroscopy in eight patients (eight to 21 positions per patient). These data were taken from the pace-mapping study previously performed by SIP-PENSGROENEWEGEN *et al.* (1990) in patients with normal cardiac anatomy. For each patient, contrast ventriculograms in the right and left anterior oblique (RAO and LAO respectively) projections were available. Three anatomical landmarks were derived from these ventriculograms by an expert cardiac electrophysiologist: the apex and the circumferences of the MVR and aortic valve ring (AVR). From the circumferences of the valves, their centres (CMVR and CAVR) were estimated. In addition, several catheter positions were determined from ventriculograms acquired during the subsequent catheter mapping procedure. The endocardial contours were also determined, but were used only for visualisation purposes.

The biplane image co-ordinates of landmarks and catheter positions, determined from the ventriculograms, were converted into 3D co-ordinates by the taking of cross-bearings.

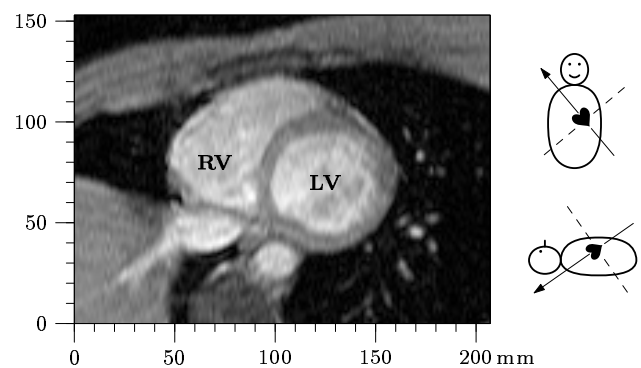


Fig. 2 Short-axis MR image from one of 24 healthy subjects (male, age 37 years). Slice was taken perpendicularly to cardiac long axis and is indicated by broken line in two schematic torso diagrams on the right. Long axis is indicated by arrow. Image was taken during end-diastole. 151×112 -pixel area is shown. Pixel diameters are 1.37 mm; this area is 207×153 mm. Bright areas are blood masses. Bright circular area in middle of image is left ventricle (LV). LV wall and interventricular septum are well discernible, but thin right ventricular (RV) free wall cannot be recognised

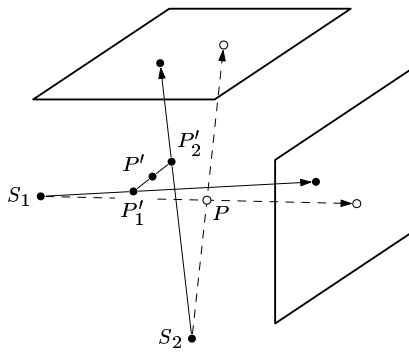


Fig. 3 Reconstruction of point from biplane ventriculograms. Actual point P is indicated; broken lines indicate correct projection of P from two X-ray sources S_1 and S_2 on detectors. Owing to measurement errors, drawn lines are measured instead. Because these lines do not cross in 3D space, shortest segment $P'_1P'_2$ that connects them is computed. Midpoint of this segment, P' , is used as an estimate for P

First, a point was identified in both images. Then, the two projection lines from the X-ray sources to the detectors were specified and their intersection point was determined. Owing to measurement errors, these lines can fail to cross. Therefore, the intersection point was approximated by taking the midpoint of the shortest line segment $P'_1P'_2$ that connects the two projection lines. This is illustrated in Fig. 3. The length of $P'_1P'_2$ was used to estimate the accuracy of the measurements; median values were 3 mm for catheter positions and 4 mm for the anatomical landmarks (CMVR, CAVR, and apex).

3 Methods

3.1 Fitting ellipsoids

The first model, a full ellipsoid of revolution, was fitted to each MRI data set by minimisation of the RMS distance between the vertices of the triangulated endocardium and the model surface, as illustrated in Fig. 4. This ellipsoid was constrained to have one aphelion located at a vertex designated the LV apex. The part of the ellipse that would cover the data points could be freely chosen by the fitting algorithm. The model parameters were the semi-major axis a and the semi-minor axis r . These parameters determine an ellipsoid obtained by rotating an ellipse around the apex–CMVR axis. The semi-minor axis of the ellipse is referred to as the ‘radius’ of this model.

The second model of the LV endocardium consisted of one-half of an ellipsoid of revolution, also with its aphelion located at the apex. In contrast to the first one, this model had its centre at a fixed position, coincident with the CMVR (Fig. 5). It follows that the semi-major axis a of this model is equal to the CMVR–apex distance. With a thus fixed, the radius r was obtained by fitting the model to the vertices of the triangulated endocardium through minimisation of the RMS distance between the vertices and the model. The optimum radius is referred to as r_f .

3.2 Testing

As the results of the fitting procedures indicated that model 2 did not perform worse than model 1, and it is more convenient because its semi-major axis a can be easily determined from the fluoroscopic data, we selected model 2 for further testing. It was tested for clinical applicability using actual biplane ventriculograms (see Section 2). The semi-major axis a was made

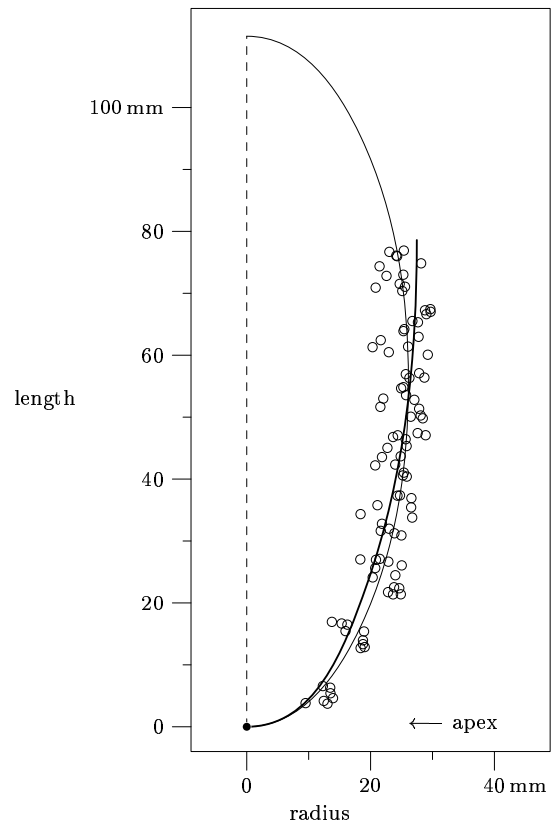


Fig. 4 Ventricular radius plotted against ventricular-length coordinate, for set of vertices of triangulated left-ventricular (LV) endocardium obtained from MRI data of one of the 24 healthy subjects (male, age 27 years). Full ellipse (model 1, thin line) and half ellipse (model 2, thick line) are fitted to these data. As azimuthal angle plays no role here, ellipsoids were ‘collapsed’ to one angle in this Figure. Thus only a half cross-section is shown. 70% of full ellipse is used in this case. Full ellipse has slightly smaller radius r than half ellipse

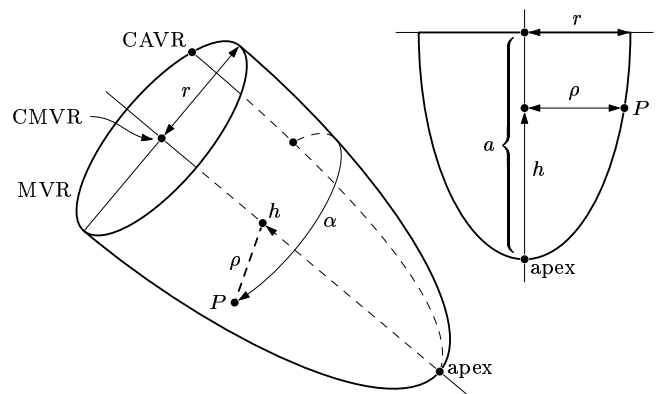


Fig. 5 Second model consists of half ellipsoid: one half of surface of revolution with elliptical cross section. Apex, mitral valve ring (MVR), centre of MVR (CMVR), centre of aortic valve ring (CAVR), parameters a and r of ellipse, and co-ordinates α and $h = la$ of an arbitrary point P are indicated. Right panel shows cross-section of model through axis and point P

equal to the CMVR–apex distance. The radius was determined in two ways

- (i) as the estimated radius of the MVR r_m
- (ii) as the CMVR–CAVR distance r_a

The results for these two methods were subsequently compared. From the 3D co-ordinates of the catheter positions obtained from biplane ventriculograms, LVCC were computed

(SIPPENSGROENEWEGEN *et al.*, 1990). The LVCC (length ℓ and azimuth α) were projected on the model surface by computation of the intersection point of the model surface and the line determined by ℓ and α . The localisation errors, defined as the distances between the positions thus estimated and the measured positions, were computed. As we could not infer absolute distances from our fluoroscopic data, we expressed the error in the 3D co-ordinates as a fraction of the individual ventricular length (the distance between apex and CMVR), multiplied by 80 mm, which is a typical ventricular length, to obtain error estimates in millimetres. For visualisation purposes the LAO and RAO projections were computed from the reconstructed 3D co-ordinates by simulation of X-ray projections.

The model was tested in a similar way on the MRI data, using the vertices of the triangulation as a substitute for catheter positions.

4 Results

4.1 Fitting the full-ellipsoid model

A full ellipsoid was fitted to each of the 24 MRI data sets. As there was no penalty for model parts that were far from the data points, the fitting algorithm was free to choose the optimum section of the ellipsoid to use; only the aphelion and major-axis direction were fixed. This optimum part of the ellipsoid was expressed as the projection of the most basal data point on the axis, normalised by the semi-major axis a . This value had mean and standard deviations of 0.5 ± 0.2 (range 0.1–0.8), indicating that the data sets resembled a half ellipsoid rather than a full ellipsoid. The median distance from the data points to this model, pooled over all MRI data sets, was 2.1 mm (range 0.0–13.5 mm). An example of a fitted ellipsoid is shown in Fig. 4.

4.2 Fitting the half-ellipsoid model

The half-ellipsoid model was also fitted to all MRI data sets. Fitting of the model comprised fixation of the semi-major axis a to the apex–CMVR distance and fitting the radius $r = r_f$. An example of a fitted half ellipsoid is shown in Fig. 4. The median distance from the data points to the model, pooled for all subjects, was 2.2 mm (range 0.0–14.1 mm). These values are similar to those for the fitting of full ellipsoids. As the semi-major axis of the half-ellipsoid model can be more easily determined from the data than that of the full-ellipsoid model, we concentrated on this model in the subsequent experiments.

4.3 Estimates for r

In the catheterisation laboratory, r has to be obtained from the biplane ventriculograms, as there are generally no 3D data available to fit the model. Therefore, we studied the relation between r_f , obtained from the fitting procedure, and the two estimates r_m (the MVR radius) and r_a (the CMVR–CAVR distance). As an estimate of the MVR radius, we used the average radius of the most basal short-axis cross-section in each MRI data set. Estimate r_m performed well: the difference $r_m - r_f$ was 0.0 ± 0.9 mm (range -1.6 to $+2.2$ mm). The distance between CAVR and CMVR proved to be a less accurate estimate for r_f : $r_a - r_f$ was 0.6 ± 5.0 mm (range -7.1 to $+10.5$ mm).

4.4 Testing the half-ellipsoid model

The method was evaluated using 107 catheter positions obtained from eight patients with biplane fluoroscopy. The model parameters were obtained from the ventriculograms, a being

Table 1 Localisation errors in millimetres for 8 patients. For each patient, the number N of catheter positions, median error, minimum error, and maximum error are given, for both methods of estimating parameter r (see text)

patient	N	localisation error with $r = r_a$			localisation error with $r = r_m$		
		median	min	max	median	min	max
1	8	2.0	0.8	10.2	2.3	0.4	11.7
2	12	7.6	3.1	13.5	3.6	0.0	17.9
3	14	3.2	0.3	13.5	4.7	0.5	14.3
4	10	3.8	1.1	10.1	3.5	0.1	12.0
5	10	2.1	0.7	5.1	5.6	1.7	10.7
6	21	5.3	0.4	17.1	12.2	1.4	26.0
7	16	3.1	0.7	13.4	3.5	0.3	11.6
8	16	5.8	0.8	12.4	3.8	0.0	10.2
mean	13.4	4.1	1.0	11.9	4.9	0.6	14.3
pooled	107	4.3	0.3	17.1	4.7	0.0	26.0

the distance from CMVR to apex and r being estimated using r_a and r_m . Cylinder co-ordinates were computed for the catheter positions and projected on the model. Localisation errors, i.e. distances between the positions estimated by the model and the measured positions, are listed in Table 1. In addition, the mean values of all patients and the pooled values for all positions together are given. With $r = r_a$, the median reconstruction error in 3D space for all fluoroscopic data was 4.3 mm (range 0.3–17.1 mm). When r_m was used as an estimate for the radius, the errors were larger with a median of 4.7 mm (range 0.0–26.0 mm). In Fig. 6, RAO and LAO projections of the measured and estimated catheter positions of a single patient are shown in relation to the cardiac anatomy.

For testing the model on the MRI data, the r parameter was again estimated using r_m (MVR radius) and r_a (CAVR–CMVR distance). With r_m , we obtained a median reconstruction error

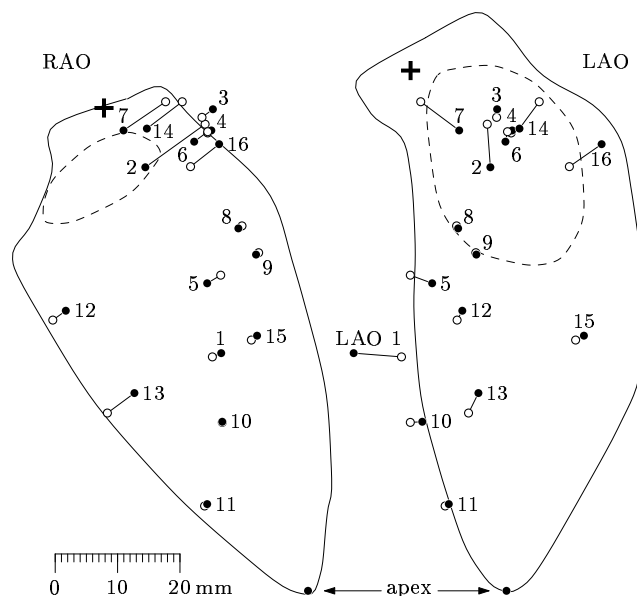


Fig. 6 Right and left anterior oblique (RAO and LAO) projections of left ventricle of patient 7 (male, age 25 years). (●) Measured catheter positions; (○) corresponding positions reconstructed from LVCCs using the half-ellipsoid model. Catheter positions are labelled with numbers from 1 to 16, to facilitate comparison of RAO and LAO data. Mitral valve ring is indicated with broken line. (+) Position of centre of aortic valve ring. Contours of left ventricle, determined with contrast cine-angiography, are shown for convenience; these contours were not used in our conversion method

of 2.2 mm (range 0.0–14.7 mm) for all MRI data sets; with $r = r_a$, the median reconstruction error was 3.5 mm (range 0.0–18.0 mm).

5 Discussion

Two simple models of the LV endocardium, a full ellipsoid of revolution and a half ellipsoid of revolution, were used to reconstruct catheter positions from LVCCs. When these models were fitted to the 3D MRI data, median fitting errors were 2 mm for both. We conclude that a half ellipsoid performs just as well as a full ellipsoid (where the used part of the ellipsoid is selected by the fitting algorithm). As the half ellipsoid can be parametrised more easily, we chose to use this model for further testing with clinical data.

A median representation error of 4.3 mm was obtained over the pooled positions of all patients when the half-ellipsoid model was tested on fluoroscopic data. The maximum error in a single patient, taken over all patients, ranged from 5 to 17 mm. These errors can be attributed in part to inaccuracies in measuring the actual catheter positions in the fluoroscopic data; these inaccuracies can be as large as 7 mm (HAUER *et al.*, 1986). Inaccuracy in the position measurement may be an important contribution to the error obtained for position 1 in patient 7 (Fig. 6). In the LAO view, the measured position lies outside the ventricular contour that was determined earlier by contrast ventriculography. This type of error can also be caused by movement of the patient during the procedure or by deformations of the endocardial wall caused by catheter pressure.

As we could not infer absolute distances from our fluoroscopic data, we had to assume a ventricular length of 80 mm for all hearts to estimate absolute reconstruction errors. For a clinical application, it would be preferable if absolute sizes could be computed. This would be feasible if the X-ray source and detector positions were known. However, absolute dimensions are not crucial for our method. Provided that the landmark positions are measured with the same system as used when catheterisation is performed, it is possible to present catheter positions on the fluoroscopy monitors, even if only relative dimensions are known.

By extracting the positions of apex, CMVR and CAVR as well as the circumference of the MVR from the MRI data sets and using the vertices of the triangulated endocardium as a substitute for catheter positions, we could also perform the testing procedure on the MRI data. Using the estimated MVR radius r_m , the median reconstruction error was 2.2 mm, which is comparable to the median residual error of the fitted half-ellipsoid model (2.2 mm). Using r_a to estimate the radius, we obtained a less accurate model with a median reconstruction error of 3.5 mm, and a larger maximum error. For the fluoroscopic data, the reverse was true: 4.3 mm median representation error with r_a and 4.7 mm with r_m as an estimate for r (Table 1). In addition, the maximum error was much larger with the latter method: 26 mm instead of 17 mm. These differences between fluoroscopic data and MRI data can be attributed to the difficulty of detecting the mitral valve contour in the ventriculograms and recognising the AVR in the MR images. However, the overall reconstruction errors of fluoroscopic data and MRI data were remarkably similar.

A VT exit site that is localised by BSM-guided pace mapping is generally used as a starting point for an activation mapping procedure aimed at identification of a suitable site for radiofrequency ablation (PEETERS *et al.*, 1999). The precise accuracy requirements for this purpose are not known. However, occasionally the exit site itself is a target for ablation. For con-

ventional radiofrequency ablation, positioning of the ablation catheter within 5 mm of the target site is required to secure a successful outcome (SIMMERS *et al.*, 1994). Although the average reconstruction errors are below this limit, 12% of the errors in the MRI data and 45% of the errors in the fluoroscopic data are larger. Application of the recently introduced cooled radiofrequency technique for VT ablation presumably does not require such a high level of reconstruction accuracy because the cooled-tip catheters produce significantly larger lesions (CALKINS *et al.*, 2000; NAKAGAWA *et al.*, 1995).

Several other models were used previously to represent the LV endocardium; an exhaustive list was given in a recent review by FRANGI *et al.* (2001). Simple models of the entire LV wall were used for simulation of cardiac excitation and recovery (LEON and HORÁČEK, 1991; NIELSEN *et al.*, 1991), but may be too inaccurate for our purpose. A bullet model was applied for LV-volume computation using echocardiography (NADKARNI *et al.*, 2000). A full ellipsoid is commonly used for contrast fluoroscopic LV volume computations (DODGE *et al.*, 1960). A half ellipsoid was previously used by GUSTAVSSON *et al.* (1993) as an initial approximation of the LV shape, which was meant to be refined with data from 2-D echocardiograms. One could also use a triangulated model of a 'standard' heart or a heart properly selected, using simple patient information, from a database such as the currently applied MRI data sets. Finally, one could fit a spline surface in three dimensions to the cardiac contours if these are available. This would require 3D echocardiography, MRI, or CT imaging prior to an ablation procedure. Electron beam computed tomography (EBCT) may be able to provide even more accurate images of the heart (DOVE *et al.*, 1994). However, in current clinical practice, usually only low-intensity biplane ventriculograms and perhaps previously created contrast cineangiograms, are available. Therefore, for our model we opted to use only the positions of the apex, CMVR and CAVR, and optionally the radius of the MVR. Still, it may be useful to develop a method that uses MRI or CT scans if they happen to be available.

In an on-line clinical application for guidance during catheter mapping and ablation of ventricular arrhythmias it may be possible to obtain catheter positions at any time from the biplane images or from other catheter localisation modalities (SHPUN *et al.*, 1997; WITTKAMPF *et al.*, 1999). If it is also known at which times the catheter tip touches the endocardial wall, this 3D position information can be used to adapt the model instantly.

We chose the fluoroscopic projections as a presentation mode because they play a key role in the electrophysiology laboratory. This allows for easy comparison of catheter positions and electrocardiographic localisation results, particularly if the data can be combined with the biplane fluoroscopic images on a single monitor.

A direct advantage of our method is that it provides a quantitative and objective alternative for a procedure that the physician now has to carry out by visually relating the LVCC provided by our electrocardiographic localisation methods to the fluoroscopic projections. In conclusion, presentation of ECG mapping data directly in biplane fluoroscopic projections provides a novel, accurate and intuitive method to guide catheter positioning and mapping prior to ablation of cardiac arrhythmias.

Acknowledgment—This work was supported by the Dutch Technology Foundation STW under grant no. AGN 66 4098.

References

- BURBANK, F., PARISH, D., and WEXLER, L. (1988): 'Echocardiographic-like angled views of the heart by MR imaging'. *J. Computer Assisted Tomography*, **12**(2) pp. 181–195.
- CALKINS, H., EPSTEIN, A., PACKER, D., ARRIA, A. M., HUMMEL, J., GILLIGAN, D. M., TRUSSO, J., CARLSON, M., LUCERI, R., KOPELMAN, H., WILBER, D., WHARTON, J. M., and STEVENSON, W. (2000): 'Catheter ablation of ventricular tachycardia in patients with structural heart disease using cooled radiofrequency energy: Results of a prospective multicenter study'. *J. Am. Coll. Cardiol.*, **35**(7) pp. 1905–1914.
- DODGE, H. T., SANDLER, H., BALLEW, D., and LORD, J. D. (1960): 'The use of biplane angiocardiology for the measurement of left ventricular volume in man'. *Am. Heart J.*, **60**(5) pp. 762–776.
- DOVE, E. L., PHILIP, K., GOTTEINER, N. L., VONESH, M. J., RUMBERGER, J. A., REED, J. E., STANFORD, W., MCPHERSON, D. D., and CHANDRAN, K. B. (1994): 'A method for automatic edge detection and volume computation of the left ventricle from ultrafast computed tomographic images'. *Investigative Radiology*, **29**(11) pp. 945–954.
- DUBUC, M., NADEAU, R., TREMBLAY, G., KUS, T., MOLIN, F., and SAVARD, P. (1993): 'Pace mapping using body surface potential maps to guide catheter ablation of accessory pathways in patients with Wolff-Parkinson-White syndrome'. *Circulation*, **87**(1) pp. 135–143.
- FRANGI, A. F., NIESSEN, W. J., and VIERGEVER, M. A. (2001): 'Three-dimensional modeling for functional analysis of cardiac images: A review'. *IEEE Trans. Med. Imaging*, **20**(1) pp. 2–25.
- GUSTAVSSON, T., PASCHER, R., and CAIDAHL, K. (1993): 'Model based dynamic 3D reconstruction and display of the left ventricle from 2D cross-sectional echocardiograms'. *Computerized Med. Imag. Graph.*, **17** pp. 273–278.
- HAUER, R. N. W., HEETHAAR, R. M., DE ZWART, M. T. W., VAN DIJK, R. N., VAN DER TWEEL, I., BORST, C., and ROBLES DE MEDINA, E. O. (1986): 'Endocardial catheter mapping: validation of a cineradiographic method for accurate localization of left ventricular sites'. *Circulation*, **74**(4) pp. 862–868.
- HOEKEMA, R., UIJEN, G. J. H., VAN ERNING, L., and VAN OOSTEROM, A. (1999): 'Interindividual variability of multilead electrocardiographic recordings: Influence of heart position'. *J. Electrocardiol.*, **32**(2) pp. 137–148.
- LEON, L. J. and HORÁČEK, B. M. (1991): 'Computer model of excitation and recovery in the anisotropic myocardium. II. Excitation in the simplified left ventricle'. *J. Electrocardiol.*, **24**(1) pp. 17–31.
- NADKARNI, S. K., BOUGHNER, D. R., DRANGOVA, M., and FENSTER, A. (2000): 'Three-dimensional echocardiography: Assessment of inter- and intra-operator variability and accuracy in the measurement of left ventricular cavity volume and myocardial mass'. *Phys. Med. Biol.*, **45** pp. 1255–1273.
- NAKAGAWA, H., YAMANASHI, W. S., PITHA, J. V., ARRUDA, M., WANG, X., OHTOMO, K., BECKMAN, K. J., MCCLELLAND, J. H., LAZZARA, R., and JACKMAN, W. M. (1995): 'Comparison of in vivo tissue temperature profile and lesion geometry for radiofrequency ablation with a saline-irrigated electrode versus temperature control in a canine thigh muscle preparation'. *Circulation*, **91**(8) pp. 2264–2273.
- NIELSEN, P. M. F., LE GRICE, I. J., SMALL, B. H., and HUNTER, P. J. (1991): 'Mathematical model of geometry and fibrous structure of the heart'. *Am. J. Physiol.*, **260** pp. H1365–H1378.
- PEETERS, H. A. P., SIPPENSGROENEWEGEN, A., WEVER, E. F. D., RAMANNA, H., LINNENBANK, A. C., POTSE, M., GRIMBERGEN, C. A., VAN HEMEL, N. M., HAUER, R. N. W., and ROBLES DE MEDINA, E. O. (1999): 'Clinical application of an integrated 3-phase mapping technique for localization of the site of origin of idiopathic ventricular tachycardia'. *Circulation*, **99** pp. 1300–1311.
- POTSE, M., LINNENBANK, A. C., PEETERS, H. A. P., SIPPENSGROENEWEGEN, A., and GRIMBERGEN, C. A. (2000): 'Continuous localization of cardiac activation sites using a database of multichannel ECG recordings'. *IEEE Trans. Biomed. Eng.*, **47**(5) pp. 682–689.
- SHUN, S., GEPSTEIN, L., HAYAM, G., and BEN-HAIM, S. A. (1997): 'Guidance of radiofrequency endocardial ablation with real-time three-dimensional magnetic navigation system'. *Circulation*, **96** pp. 2016–2021.
- SIMMERS, T. A., WITTKAMPF, F. H. M., HAUER, R. N. W., and ROBLES DE MEDINA, E. O. (1994): 'In vivo ventricular lesion growth in radiofrequency catheter ablation'. *PACE*, **17** pp. 523–531.
- SIPPENSGROENEWEGEN, A., SPEKHORST, H., VAN HEMEL, N. M., KINGMA, J. H., HAUER, R. N. W., JANSE, M. J., and DUNNING, A. J. (1990): 'Body surface mapping of ectopic left and right ventricular activation: QRS spectrum in patients without structural heart disease'. *Circulation*, **82** pp. 879–896.
- SIPPENSGROENEWEGEN, A., SPEKHORST, H., VAN HEMEL, N. M., KINGMA, J. H., HAUER, R. N. W., JANSE, M. J., and DUNNING, A. J. (1992): 'Body surface mapping of ectopic left ventricular activation: QRS spectrum in patients with prior myocardial infarction'. *Circ. Res.*, **71**(6) pp. 1361–1378.
- WITTKAMPF, F. H. M., WEVER, E. F. D., DERKSEN, R., WILDE, A. A. M., RAMANNA, H., HAUER, R. N. W., and ROBLES DE MEDINA, E. O. (1999): 'LocalLisa: New technique for real-time 3-dimensional localization of regular intracardiac electrodes'. *Circulation*, **99** pp. 1312–1317.

Author's biography

Mark Potse received the MSc degree in physics in 1996, and expects to receive the PhD degree in December 2001, both from the University of Amsterdam, The Netherlands. From 1996 to 2001 he was employed as a PhD student, supported by a grant from the Technology Foundation STW, at the Medical Physics department, University of Amsterdam, on a project for the real-time analysis of body surface maps. Since 2001 he has been employed as a research assistant at the same department. His research interests include multichannel ECG analysis, software development, and cardiac electrophysiologic modeling.